Supporting Information for

Petro-mineralogical controls on coda attenuation in volcanic rock samples

María Del Pilar Di Martino[1,3], Luca De Siena[2], David Healy[1], and Stephanie Vialle[3]

[1]School of Geosciences, University of Aberdeen, Aberdeen, UK.

[2]Institute of Geosciences, Johannes Gutenberg University Mainz, Mainz, Germany.

[3]WASM: Mineral, Energy and Chemical Engineering, Curtin University, Perth, Australia.

Content

This file contains supplementary information separated into seven sections:

S1. Porosity and velocity measurements: Table **S1**, Figures **S1.1** and **S1.2**

S2. Rock-physics cross-plots: Figure **S2**

S3. Ultrasonic experiments: Figures **S3.1**, **S3.2** and **S3.3**

S4. Selection of the coda window: Figure **S4.1, S4.2, S4.3** and **S4.4**

S5. Thin section images: Figure **S5**

S6. Mineral distribution per sample: Figure **S6**, Tables **S6.1**, **S6.2** and **S6.3**

S7. Statistical parameters computed for each sample: Table **S7**

S8. Qc versus frequency content. Figures **S8.1**, **S8.2** and **S8.3**

References not cited in the manuscript:

ASTM (2000) American Society for Testing and Materials. Annual book of ASTM standards, vol 04.08, Philadelphia, PA, USA

Ji, S., Shao, T., Michibayashi, K., Long, C., Wang, Q., Kondo, Y., et al., (2013). A new calibration of seismic velocities, anisotropy, fabrics, and elastic moduli of amphibole-rich rocks: Seismic properties of amphibolites. *Journal of Geophysical Research: Solid Earth, 118*(9), 4699–4728. https://doi.org/10.1002/jgrb.50352

Lebedev, M., Bóna, A., Pevzner, R., & Gurevich, B. (2011). Elastic anisotropy estimation from laboratory measurements of velocity and polarization of quasi-P-waves using laser interferometry. *Geophysics*, *76*(3), WA83–WA89. https://doi.org/10.1190/1.3569110

S1 - Porosity and velocity measurements

The sample preparation and initial description was performed by VBPR (Table S1). The samples were cored in the Rock Physics Laboratory at the University of Aberdeen. The specimens are cylindrical cores of around 2.54 cm in diameter and 5.08 to 6.35 cm in length. The samples ends were polished using a polishing wheel to decrease roughness and washed with water to remove any rest of particles. The length-to-diameter ratio lies between 2 to 2.5 which is consistent with the minimum aspect ratio recommended to avoid end constraint effects when measuring amplitudes in the laboratory (ASTM 2000).

Table S1. *Sample's description.*

ID	Depth m	D	Facies	Description	Secondary features	Length cm	Diameter cm	λ_{Sw} (mm)
1H	641.4	X	A	Small isolated vesicles, densely plagioclase phyric	Fresh	4.99	2.57	15.0
2H	889	X	P	Olivine phyric, dispersed irregular micro-vesicles	Fresh	4.91	2.56	6.4
3H	889	X	P	Olivine phyric, dispersed irregular micro-vesicles	Fresh	5.06	2.57	5.2
4H	954.6	X	T	Medium to large irregular vesicles, partly connected	Possible minor dissolution?	5.12	2.56	25.4
5H	1020.7	Z	A	Small aligned vesicles, elongate to irregular	Fresh	5.11	2.57	13.0
6H	1038.1	X	P	Densely olivine phyric, medium size vesicular	Mostly fresh	5.06	2.56	25.3
7H	1179.1	X	P	Moderately vesicular to amygdaloidal, medium size	Partly to completely filled vesicles	5.14	2.56	19.3
8H	1230.9	Z	P	Clay rich, minor vesicle evidence	Highly altered	5.06	2.56	8.7
9H	1686.2	Z	P	Moderately vesicular, some larger coalesced	Mostly fresh, pale grey vesicle coatings	5.10	2.56	15.0
10H	1686.2	Z	P	Moderately vesicular, some larger coalesced	Mostly fresh, pale grey vesicle coatings	5.05	2.55	12.5
11H	1689.7	X	P	Densely vesicular, small, minor coalescence	Mostly fresh, rare zeolite fills(detached)	4.98	2.55	12.1
12H	1716.4	X	P	Large mostly isolated vesicles	Weakly altered to fresh, rare zeolite filled vesicles	5.07	2.56	9.1

13H	1716.4	X	P	Large mostly isolated vesicles	Weakly altered to fresh, rare zeolite filled vesicles	4.99	2.56	12.8
14H	1727.9	Z	P	Medium isolated vesicles	Weakly altered, zeolite coating/partial fill	4.99	2.56	10.6
15H	1729.6	Z	P	Medium to large irregular vesicles	Weakly altered around vesicle rims	4.88	2.57	13.4
16H	1729.6	Z	P	Medium to large irregular vesicles	Weakly altered around vesicle rims	4.97	2.56	14.1
17H	1738	Z	P	Massive medium crystalline	Weakly altered	5.07	2.56	11.2
18H	1747.8	Z	P	Medium-sized moderately vesicular	Partial to complete zeolite fills, highly altered	4.44	2.57	15.2
19H	337.5	Z	A	Small to medium vesicles, olivine phyric	Fresh	6.30	2.56	18.9
20H	692.8	X	P	Highly vesicular, medium-sized	Weakly altered, possible minor dissolution?	5.12	2.56	12.5
21H	818.1	Z	P	Highly vesicular, small vesicles	Weakly altered, minor linings in places	6.47	2.55	8.6
22H	969	Z	P	Small to medium dispersed vesicles	Weakly altered	5.04	2.56	13.5
23H	1122.8	Z	P	Moderately vesicular, medium size	Moderately altered, oxidized throughout	6.39	2.56	11.0
24H	1283	Z	I	Angular fragments of basalt in altered matrix	Altered	5.09	2.55	11.2
25H	1456.7	Z	P	Moderate to densely vesicular, mostly detached	Weakly altered, trace oxidation throughout	6.54	2.56	9.8

Note. Column 'D' refers to the direction of the core plugs: 'Z' perpendicular and 'X' parallel to the main core axis, respectively. The facies are A: Aa lava and P: Pahoehoe lava.
Column λ_{Sw} refers to the S-wave wavelength computed at the individual central frequency recorded at the ultrasonic waveform for each sample.

Petrophysical properties were measured on the cored samples at ambient room temperature (~18-20℃) and atmospheric pressure (1 bar). To measure the porosity of the core plugs a Helium porosimeter was used: the core plug is put into a tight chamber, a known volume of Helium gas is injected (from a different chamber) at a defined pressure, then the equilibrium pressure of the two chambers is recorded, allowing to determine the grain volume. The calliper measurements are used to generate the volumes of the core plug, making it possible to calculate the bulk and grain density and porosity, such that:

$$Bulk\ Density = \frac{Weight\ (g)}{Bulk\ volume\ (cc)}$$

$$Grain\ Density = \frac{weight\ (g)}{Bulk\ volume\ (cc) * (1 - \frac{Pore\ volume\ (\%)}{100})}$$

$$Porosity\ \% = \frac{Bulk\ volume - Grain\ volume}{Bulk\ volume} * 100$$

As part of this study, we also estimated porosity from the polished thin sections (2D). Two different methods were used: (1) binary segmentation of the light microscopy images using ImageJ software; and (2) manual segmentation of BSE images using Aviso software. The computed porosity values were close and comparable with the 3D porosity measured in the rock samples (RP-plug) (Fig. S1.1); the higher differences observed in sample 4H between the measured and computed values are likely due to the large vesicles of the sample that make it quite heterogeneous at the core scale (Fig. S5). These results give us confidence to extrapolate analysis done on the thin sections (2D) as a reliable representation of the sample (3D).

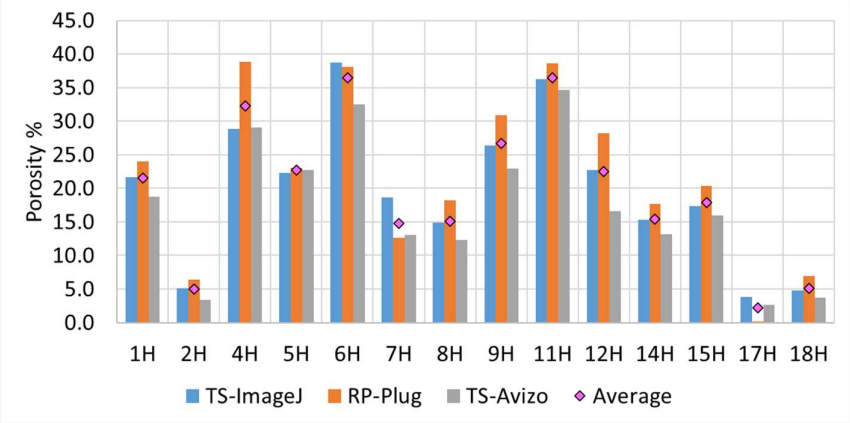

Figure S1.1. *Porosity in the sample obtained by three different methods and its average; computed from 2D images (TS-ImageJ and TS-Avizo) and measured in the laboratory on the 3D core plugs (RP-plug).*

Velocity estimation.

The samples were oven-dried at 40 ℃ for about 24 hours before acquiring ultrasonic waveforms. We measured ultrasonic velocities (see section 3.1 of the main manuscript for details on the acquisition system). The induced *P* wave was straightforwardly identified as the first break on the waveforms (Pa in Fig. S1.2). To pick the *S* wave arrivals (Sa), we changed the polarization of the transducer in three different settings: (1) with the transducers aligned, (2) with the source transducer rotated by 90 degrees (around its own axis), and (3) after inverting the sample to change the source/receiver position. The picked arrival times are corrected to account for the natural delay of the electronics. The velocity of the phases was calculated then by dividing the length of the samples by the wave-arrival time.

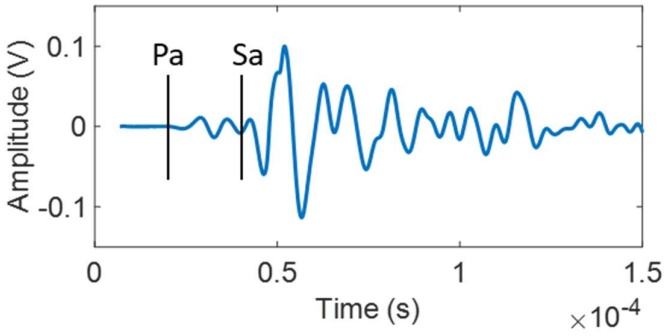

Figure S1.2. *Picking of P- (Pa) and S- wave (Sa) arrival times on the ultrasonic waveform recorded in sample 1H.*

S2 – Rock Physics cross-plot

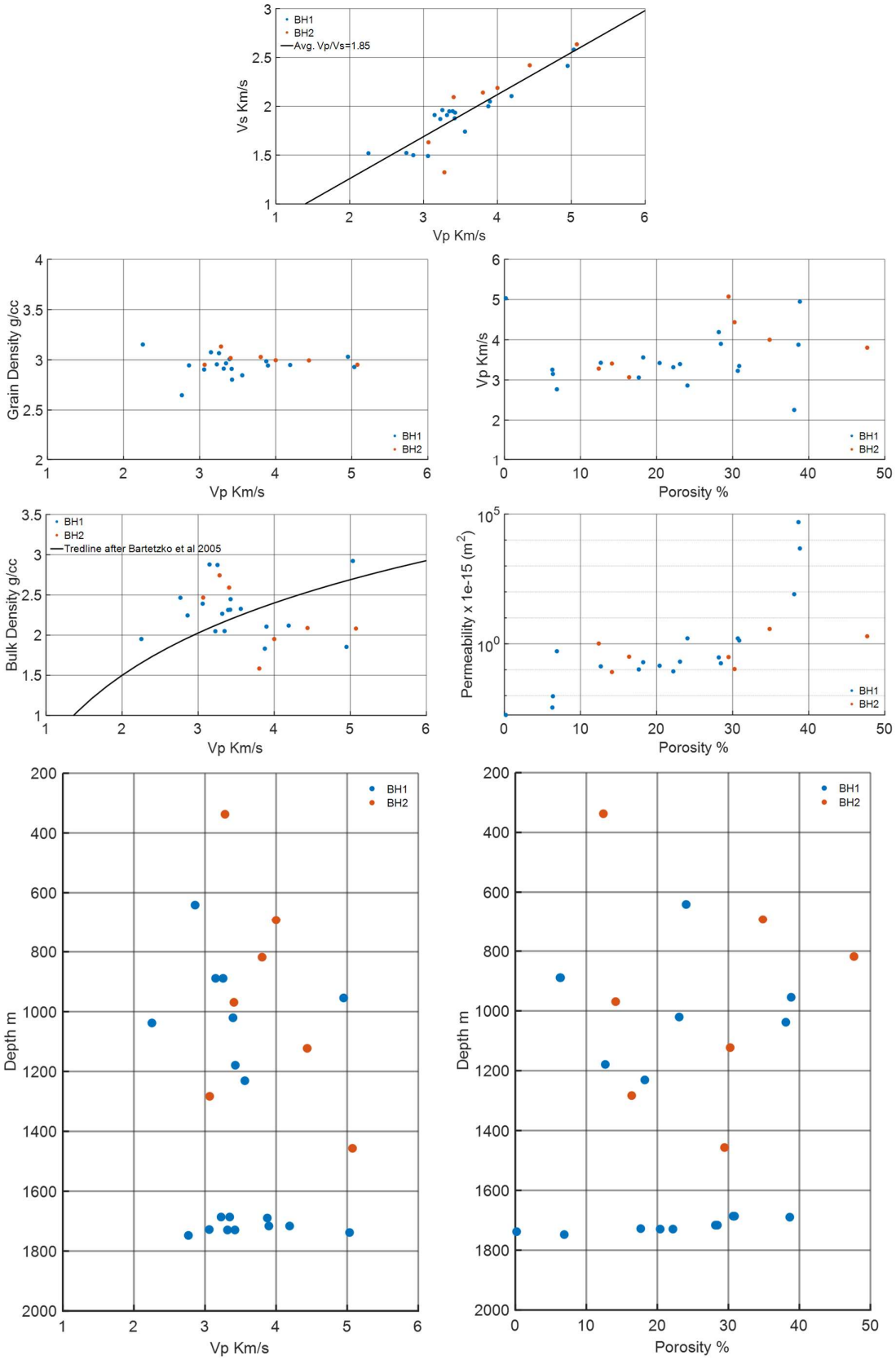

Figure S2. *Cross-plots of rock physics properties in the samples*.

S3 – Laboratory Experiments to record coda waves

The seismic survey was performed at the Rock Physics laboratory of the University of Aberdeen and the Rock Physics laboratory of Curtin University.

3.1 Influence of electronics

A test was done to evaluate the influence of the acquisition parameters in the coda-attenuation values; it was found that inputs such as the pulser voltage (amount of voltage that provides power to the pulser and allows to maintain a constant source amplitude) and the receiver gain (that controls the amplification/attenuation of signals processed by the receivers) must be constant for all the measurements because small changes in these values dramatically affect the propagation of the signal in the coda part of the waveform. The waveforms for *P*- and *S*- waves were re-acquired for the core samples after selecting common input parameters for the acquisition, to guarantee consistency when comparing results between datasets.

3.2 The assembly of the experiment

The samples were placed in vertical position (its long axis) into a chamber that secured the source and receiver transducers, located at the top and bottom side-ends of the sample, respectively. Two experimental set-ups were tested (Fig. S3.1):

(1) Near ambient confining pressure was applied by tightening the core chamber; through finger-tight of butterfly screws. This approach causes variations in the waveform due to inconsistencies in the pressure applied to hold the core in the chamber (Fig. S3.1a). For this reason, it was decided to use a torque wrench to apply a constant force on the top bolt to ensure good transducer-sample coupling; however, the error associated with the repeatability of the experiment is still considerable.

(2) The transducers were placed in a box-holder coupled to an internal spring to guarantee equal pressure conditions, as it allows the coupling force to be independent of the assembly system (Fig. S3.1b). To ensure repeatability, these holders were attached to a bracket system to give stability and to hold the sample in the middle of both transducers while keeping them aligned.

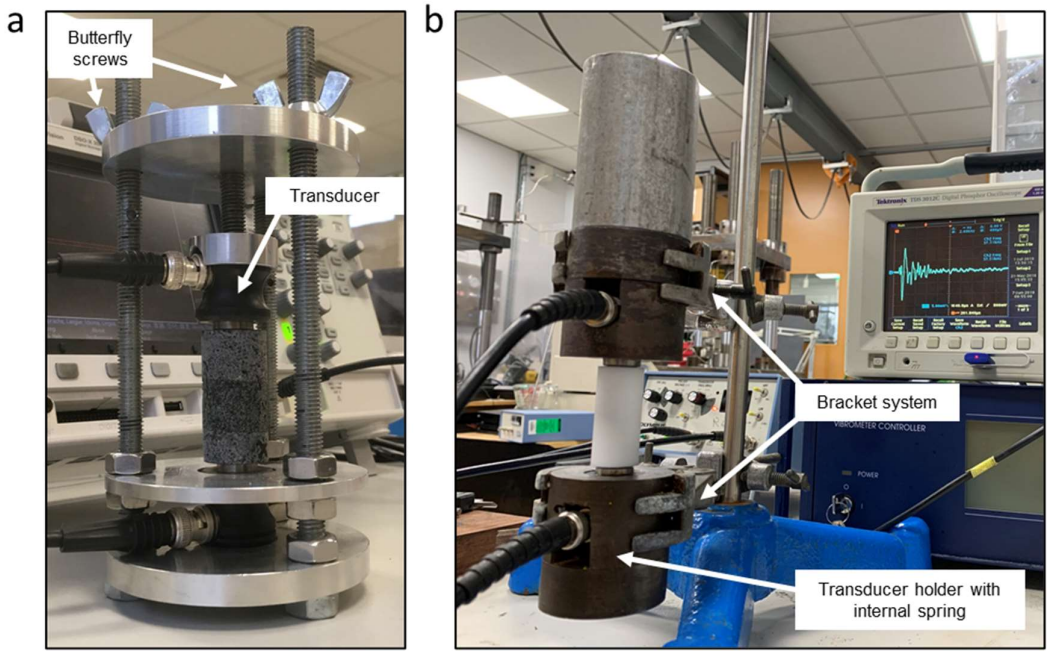

Figure S3.1. *Experimental set-up for the acquisition of ultrasonic waveforms at the rock physics laboratories of the University of Aberdeen* (a) *and Curtin University* (b), *note the aluminium block in* (b) *is not applying any force to the transducer, was only used to check the equilibrium of the holder-transducer-sample system.*

3.3 The coupling sample transducer

To achieve a good signal propagation without the need of applying pressure to pair the assembly, it was decided to glue the *P* wave transducers to both sides of the samples. In this case, we worked with the *P* wave transducers because their diameter coincided with the diameter of the samples of 1 inch. The glue applied was common 'super-glue', the sample-transducer was left to dry for a couple of hours and then the measurements were acquired. It resulted in a good strategy for measuring *P* wave arrival times. However, we stopped using this approach because: (1) the characteristics of the transducers (Accuscan type, characterized by a narrow bandwidth and limited axial resolution) were inappropriate to record long signals accurately, forbidding coda analysis; and (2) it was necessary to immerse samples and transducers in acetone overnight to separate them, which could damage both the sample and equipment.

The *S* wave transducers used are of the type Videoscan, which are advised for attenuating or scattering materials. We tried to improve the contact between these transducers and the sample by adding Treacle syrup to the side-ends of the core samples. We did not notice any improvement on the waveforms.

3.4 The LDI method

Laser Doppler Interferometer (LDI) is a relatively new non-invasive method for measuring *P* and *S* wave velocities in rock sample (Lebedev et al. 2011). A piezoelectric transducer is used as the source while the LDI measures the velocity (or displacement) at the surface of the sample in a small area (micrometer scale) along the direction of the laser beam. The apparatus used allows measuring velocity at a frequency range of 2.5 MHz. To generate a source an *S* wave transducer was coupled to the bottom side of the cylindrical sample (located in vertical axis direction). A reflective tape was glued at the top side of the sample to reflects light backwards, then the vibration was detected by the LDI. The measurements were made at the centre of the sample. (Fig. S3.2). Unfortunately, most of the core samples in our dataset are extremely attenuative making it impossible to achieve a good signal-to-noise ratio to acquire a good waveform.

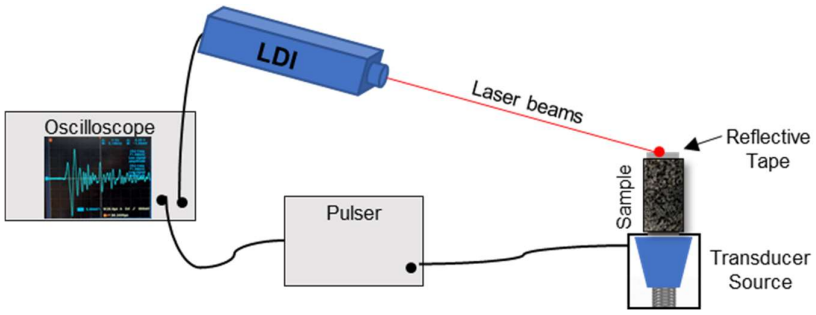

Figure S3.2. *Schematic illustration of the experimental set-up for the LDI measurements.*

3.5 The stress associated method

To test the change in velocity and coda signals when applying pressure to the samples we devise and experiment using a hook cell that allows applying axial and confining pressure simultaneously to the samples (Fig. S3.3). As the idea was to preserve the conditions of the samples (i.e. we do not want to generate new cracks), the confining pressure and maximum axial pressure (to keep the equilibrium state) was computed by considering the initial hydrostatic pressure from the depth where the cores were extracted. The available equipment was designed to work with samples twice the diameter size of the core plugs (2 inches), then it was necessary to create a 'rubber' jacket to: (1) hold the sample, (2) fit the space in the pressure chamber and (3) improve boundary conditions by absorbing coherent waves at the boundaries of the sample.

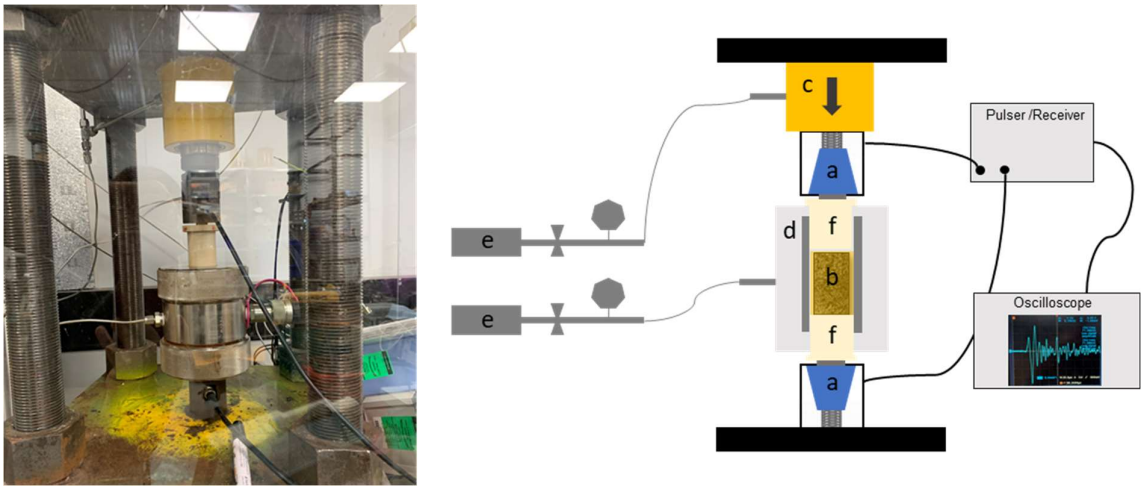

Figure S3.3. *Schematic of the experiment. a: transducer in box holder with spring attached; b: jacketed rock sample; c: hydraulic uniaxial; d: sample chamber with confining stress; e: pressure control; f: Piston*

- *Creation of Jacket*

The material used to create the jacket is a mixture of polyether elastomer (Erapol CCM75A). The components were mixed and poured into a Teflon mould (previously created) with the dimensions of the required jacket. After allowing 1- week time for cure the casting was demoulded. Despite several attempts to avoid trapped air in the jacket, the chemical components and small pouring space created small inhomogeneity which could have effects on amplitude recordings. Rubbers jackets are known to weaken boundary reflection (Wei & Fu, 2014); however, in our case, some high-frequency resonances were generated when applying confining pressure to the jacket. This is probably due to the chemical features of our jacket. Then only uniaxial pressure was applied with low increments from 0 to 1 MPa.

S4 – Coda Window

The acquired waveforms have a length of 4e-04 seconds. We decided to use a common coda window for all the samples starting at 1.75e-04 seconds and with a length of 1.75e-04 (Fig. S4.1-a). In the envelope of the signal (Fig. S4.1-b), we noticed small increases across the decreasing coda decay. These increases are related to reverberations from the ends of the samples (seismic multiples). To understand the effect of these secondary reflections in our sample we analysed the wave propagation on an aluminium plug (Fig. S4.1-d) with dimensions similar to the rock samples. In the corresponding waveform, the reflections are evident after three times the first wave arrival, both in the envelope (Fig. S4.1-e) and in the spectrogram (Fig. S4.1-f). These multiples have high magnitudes, as expected in aluminium, which has very low attenuation. In the spectrogram of our rock sample (Fig. S4.1-c), the magnitudes of these multiples are not comparable with the magnitude of the direct wave package. Indeed, if we change the colour scale to appreciate better the magnitudes at later times, the multiples arrivals (after the first two multiples) for the rock sample are irrelevant (Fig S4.2). We thus decided to neglect the effect of these secondary increases and to choose a long coda window starting at 1.75e-04 seconds from the origin time, which is at least four times the arrival time of the S-wave. This choice allows removing the first multiple, which is by far the most intense in the coda. The second multiple is removed in 92% of the cases.

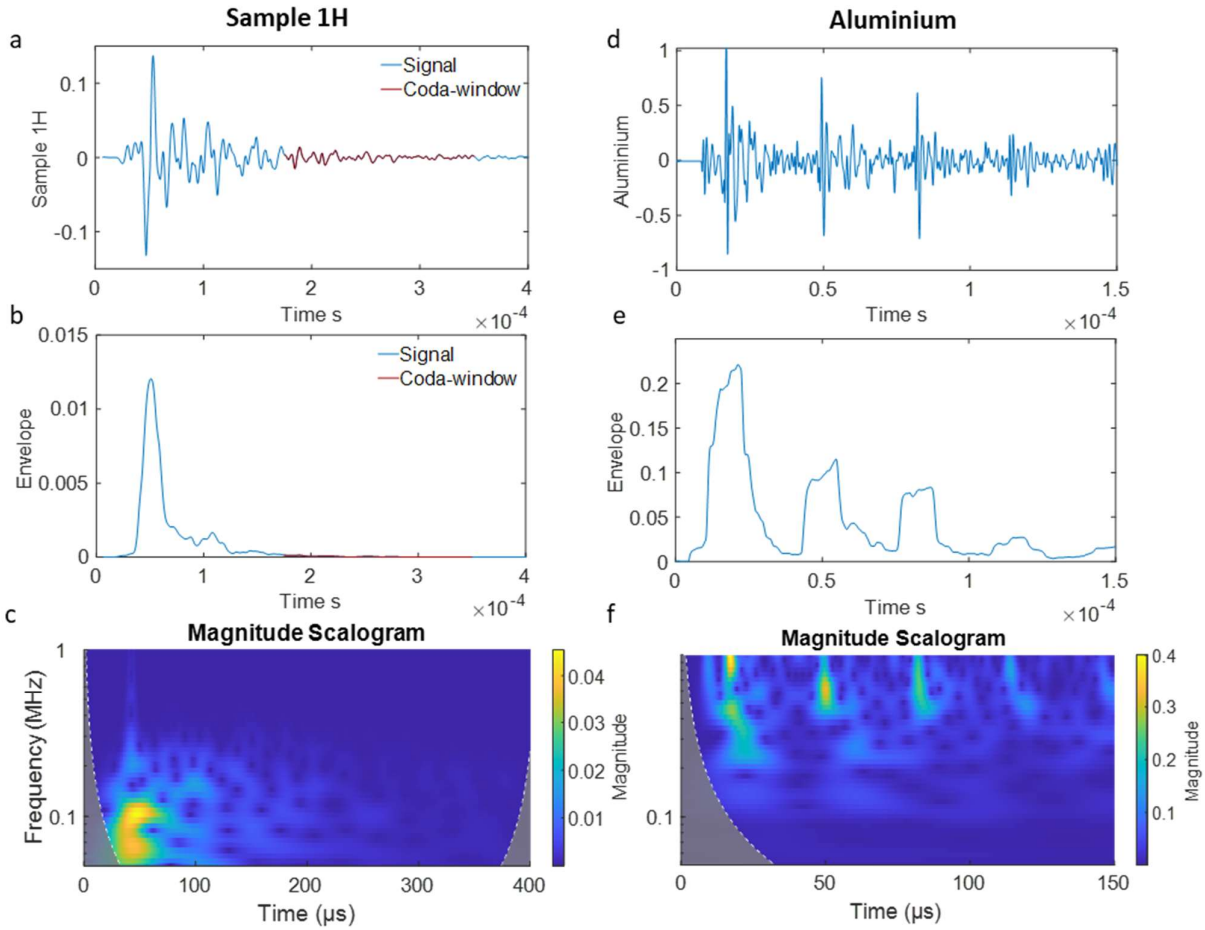

Figure S4.1. *Selection of the coda window. Ultrasonic waveform for sample 1H* (a), *its envelope* (b) *and the scalogram of the signal* (c). *Ultrasonic waveform for aluminium sample* (d), *its envelope* (e) *and the scalogram of the signal* (f).

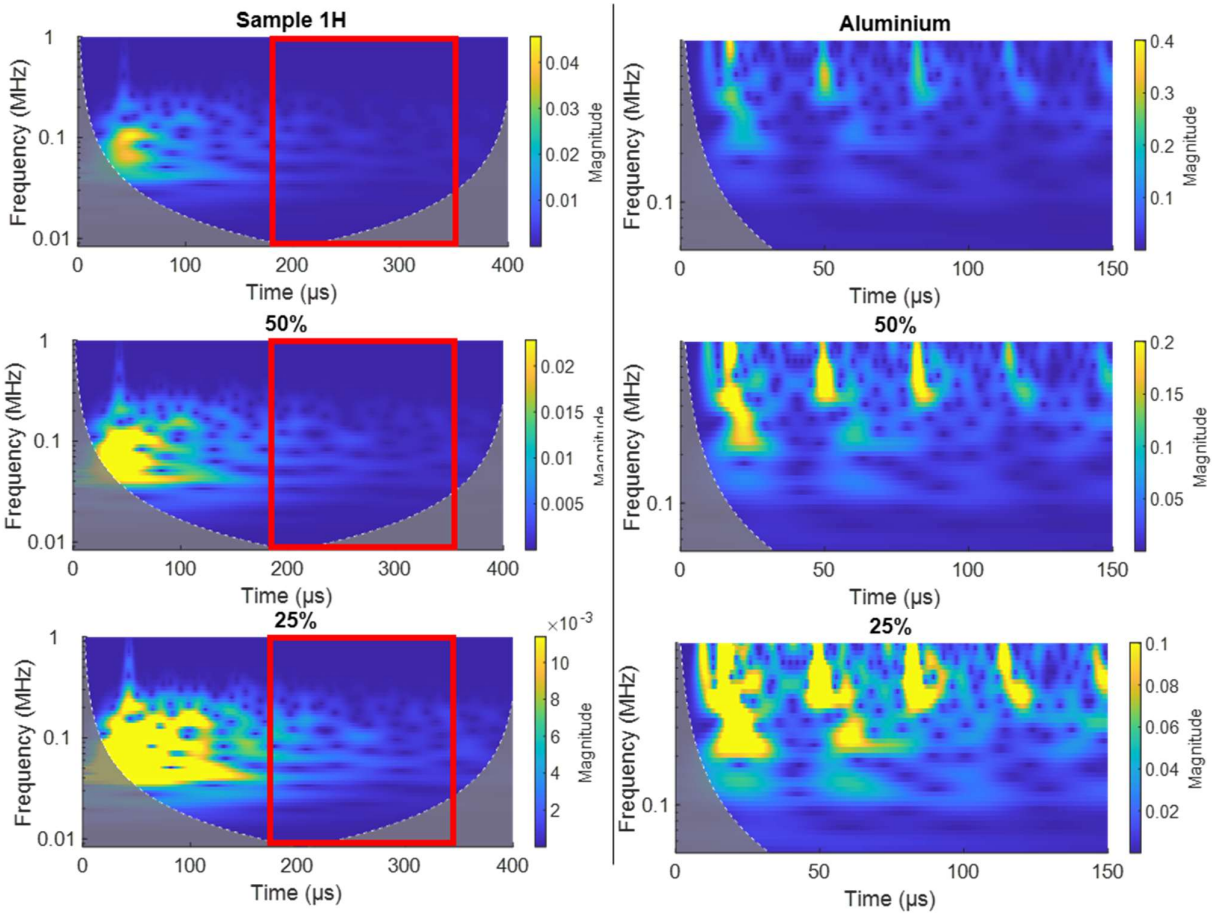

Figure S4.2. *Magnitude scalogram. Rock sample (left) and aluminium sample (right). By changing the colour scale to 50% and 25% of the maximum amplitude, the multiple arrivals are more easily visible. The coda window corresponds to the area in the red box, which does not have a noticeable influence from the multiples.*

Qc values for different coda windows selection.

Four methods were tested (e.g., sample 4H in the figure below):

1- **Fixed coda**: coda start at 175 µs and end at 350 µs for the entire dataset.
2- **Early coda**: coda window starts after the S wave package (from 50% decay of its maximum amplitude) and ends before the first multiple.
3- **S wave related coda**: coda starts after 5 times after the S wave arrival time with a fixed length of 200 µs.
4- **Maximum amplitude related coda**: coda start 4 times after the time at which the maximum amplitude of the signal occurs, with a constant length of 100µs.

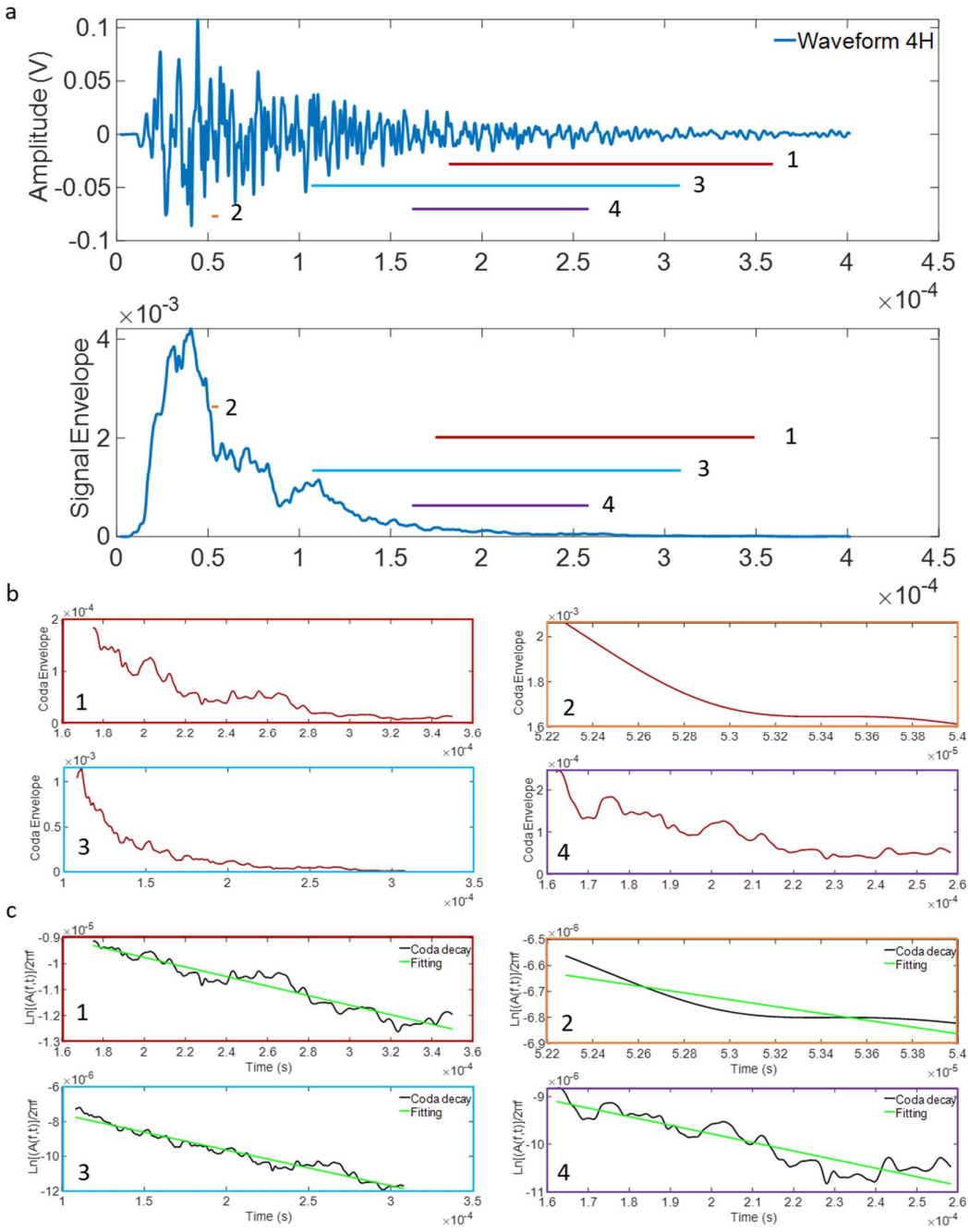

Figure S4.3. *Coda window selection and Qc computation for sample 4H.*

The early coda window approach was unsuccessful within our dataset because the coda lengths had to vary from 1.7 to 30 μs, given the different elastic properties of the samples. This is a difference of 40 to 750 data points. We consider that having less than 250 data points (10 μs window) makes the calculation of Qc unreliable.

We decided not to use the S-wave coda related window because we were not confident in the picking of the S wave arrival, which was challenging in some samples.

For the maximum amplitude related coda, the location of the coda window in the seismogram varies between samples, it goes from as early as 120-200 μs in sample 2H to as late as 300-400 μs for sample 19H. We believe this compromises the comparison between different samples.

We opted for a fixed coda window between 175 and 350 μs for the entire dataset. This window selection (1) is the best approach to be able to compare results between samples, (2) takes out the uncertainty associated with the arrival picking, (3) removes the effect of the first multiple for all the samples and it starts after the second multiple in 92% of the samples, (4) avoid the low s/n ratio at the end of the seismograms, (5) the correlation coefficient of the fitting line to compute Qc is above R=0.60 for all the samples and above R=0.80 for 60% of the samples, and (6) it is similar to the window selection approach used when analysing field data.

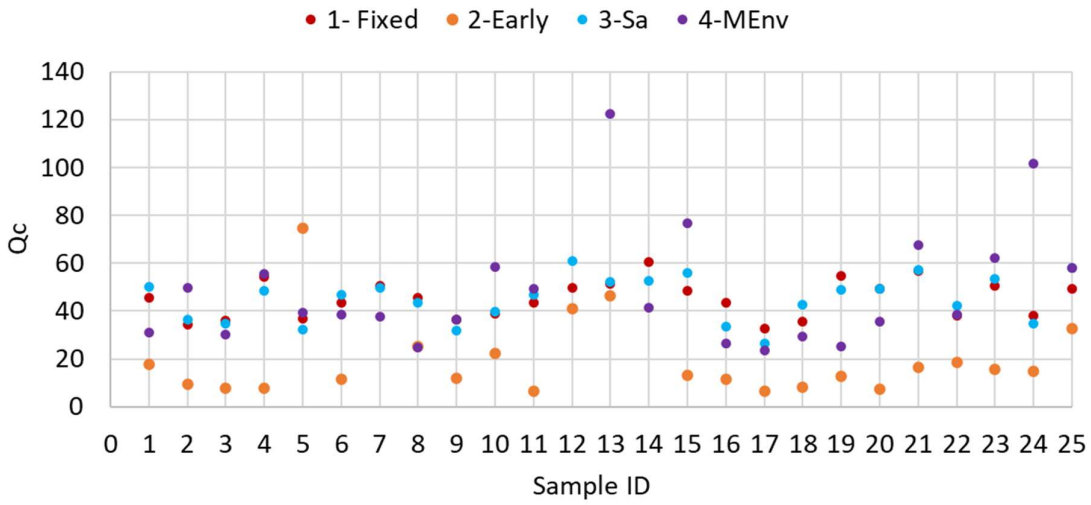

Figure S4.4. *Qc values computed for 4 coda window types (1: fixed late coda, 2: variable early coda; 3: related to S wave arrival time; 4: related to maximum amplitude in the envelope). Methods 1 and 3 gave relatively similar Qc values, both with R values above 0.60; Method 2 has outliers values for samples 7 and 14 and has 6 samples with R values lower than 0.60; Method 4 has outliers for samples 12, 13 and 24, and 10 samples with R values lower than 0.60.*

S5 – Thin sections

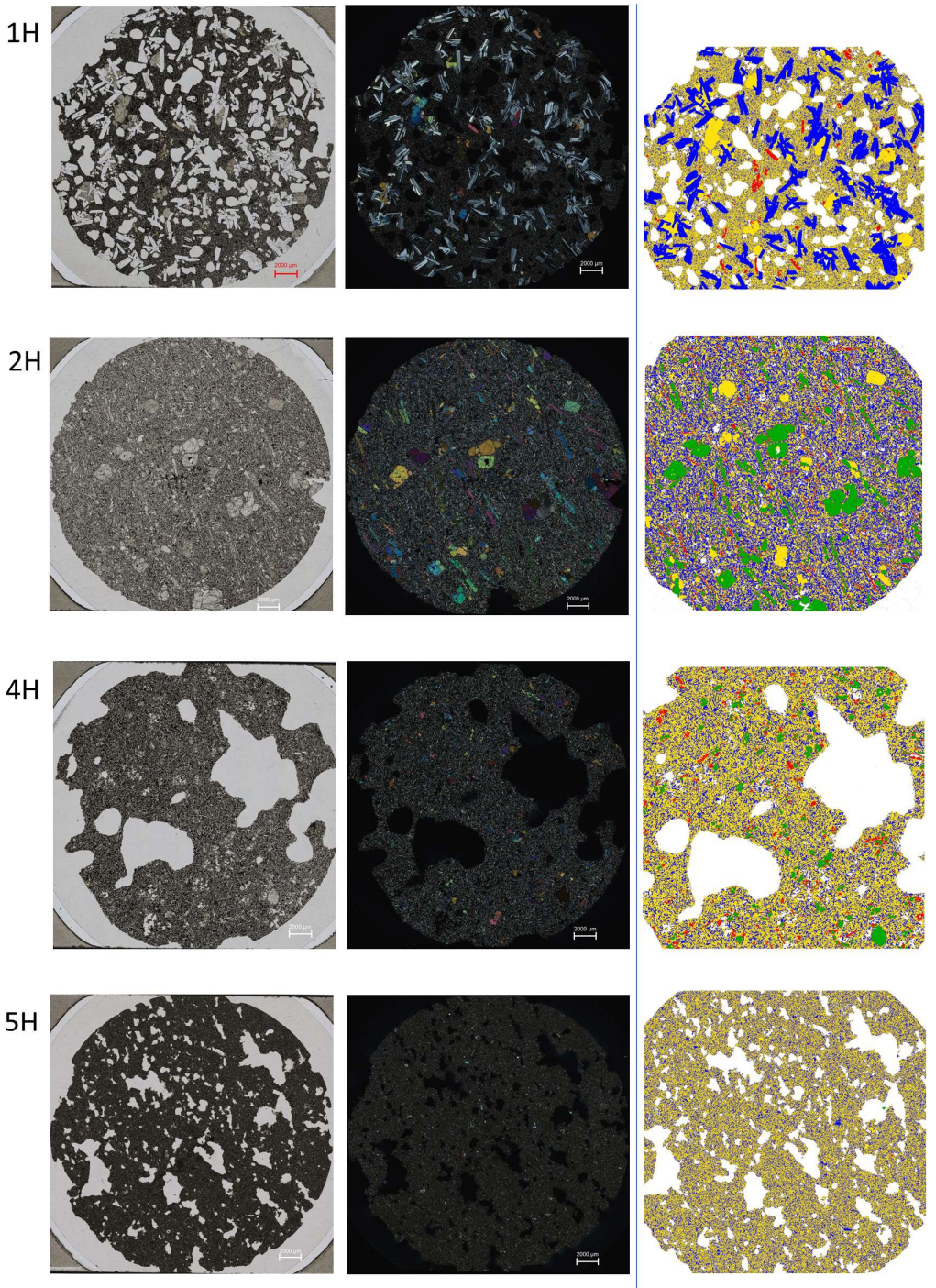

Optical images under plane polarised light (first column) and crossed-polarised (second column)

Phase identification map taken in a scanning electron microscope (TIMA system)

- Amphibole
- Feldspars
- Pyroxene
- Olivine
- Zeolites
- Others

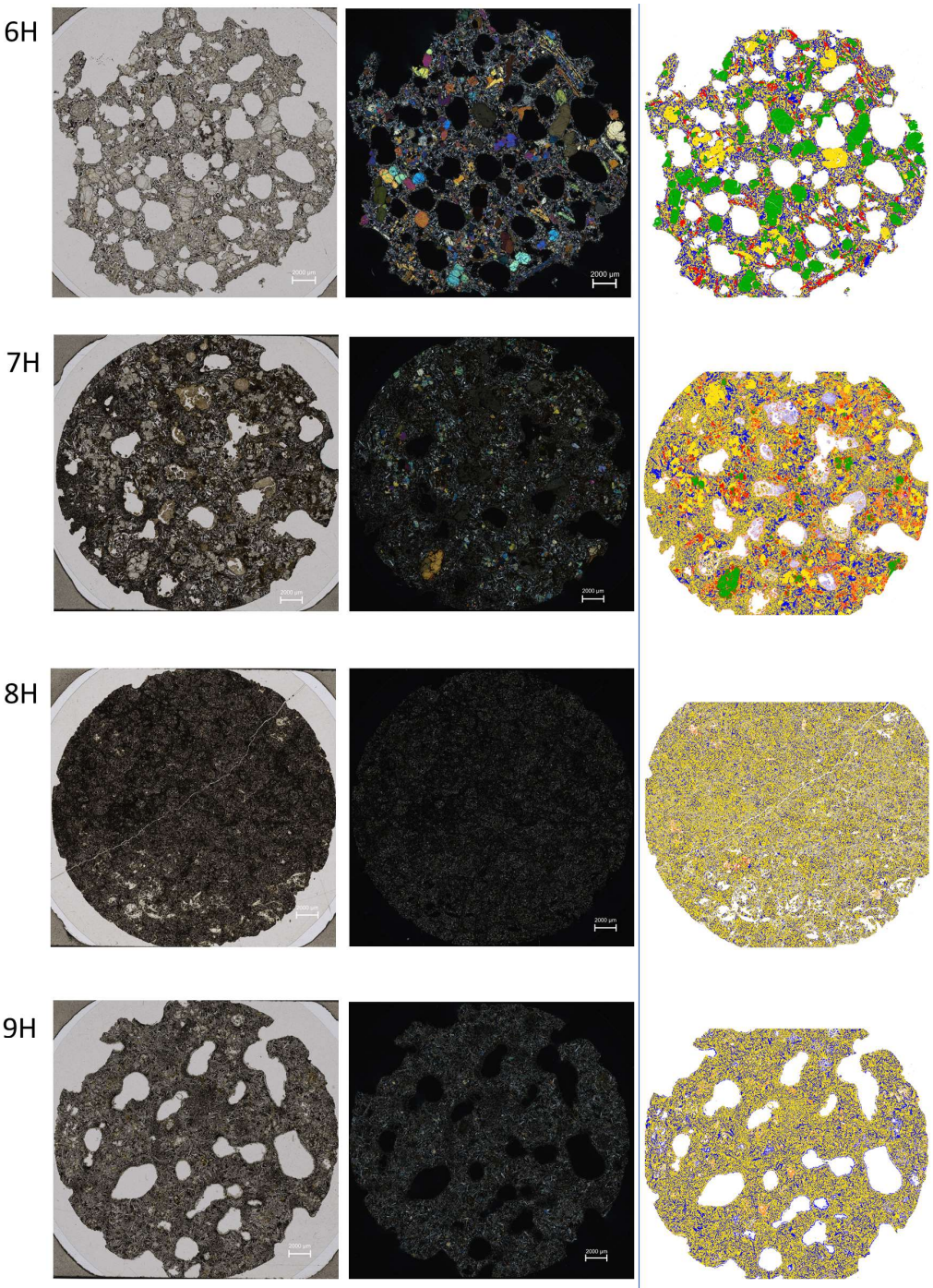

Optical images under plane polarised light (first column) and crossed-polarised (second column)

Phase identification map taken in a scanning electron microscope (TIMA system)

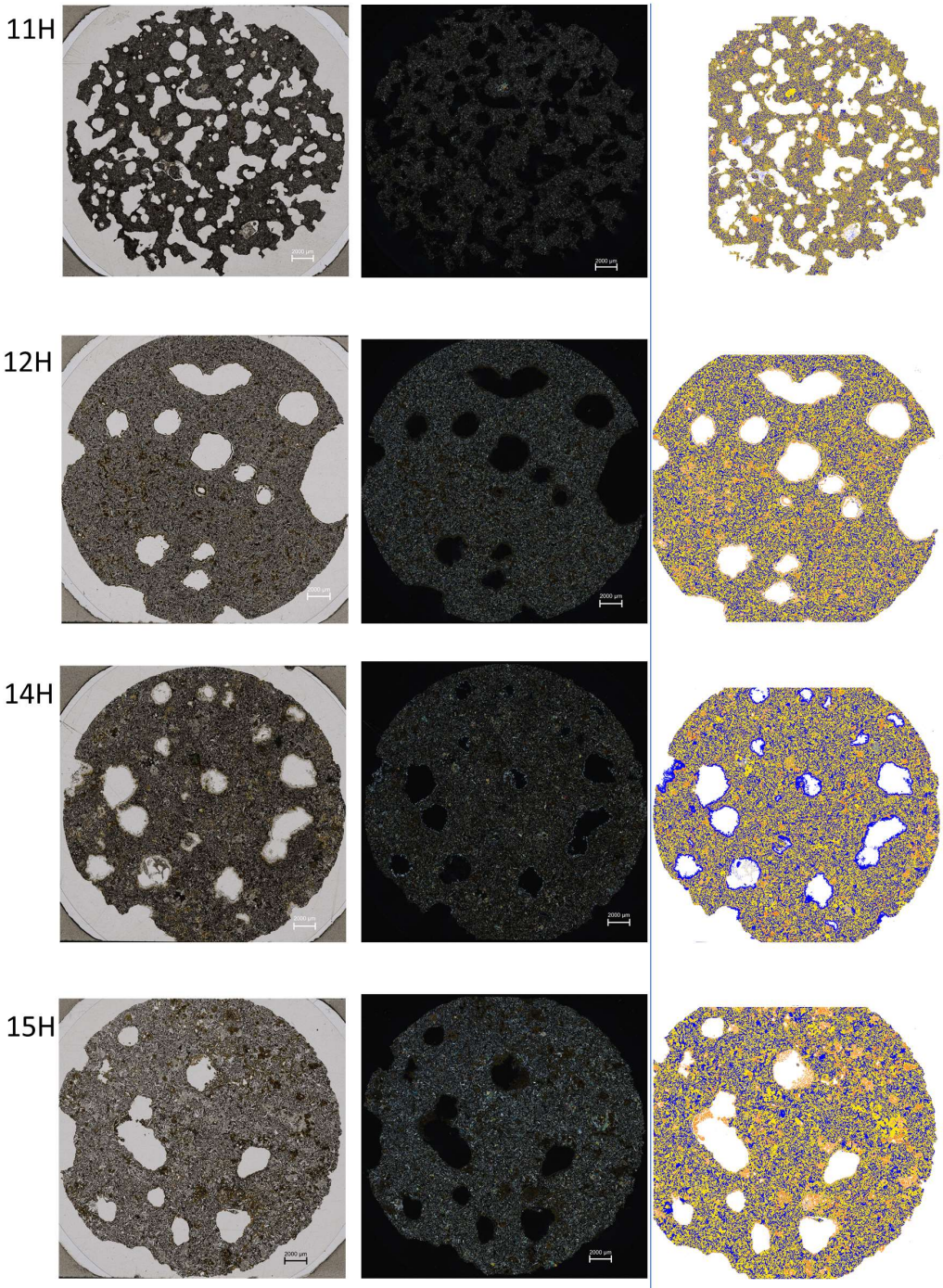

Optical images under plane polarised light (first column) and crossed-polarised (second column)

Phase identification map taken in a scanning electron microscope (TIMA system)

- Amphibole
- Feldspars
- Pyroxene
- Olivine
- Zeolites
- Others

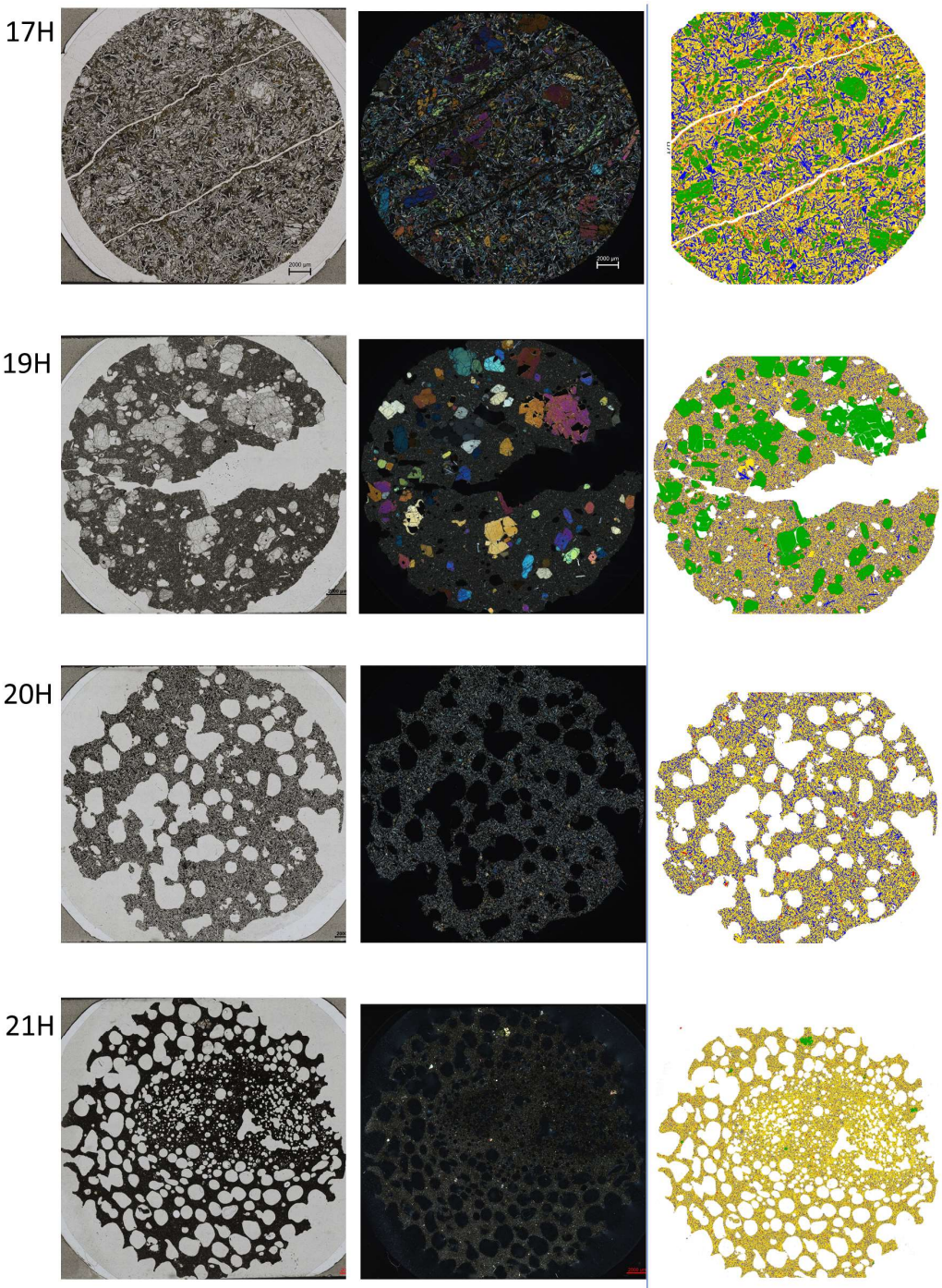

Optical images under plane polarised light (first column) and crossed-polarised (second column)

Phase identification map taken in a scanning electron microscope (TIMA system)

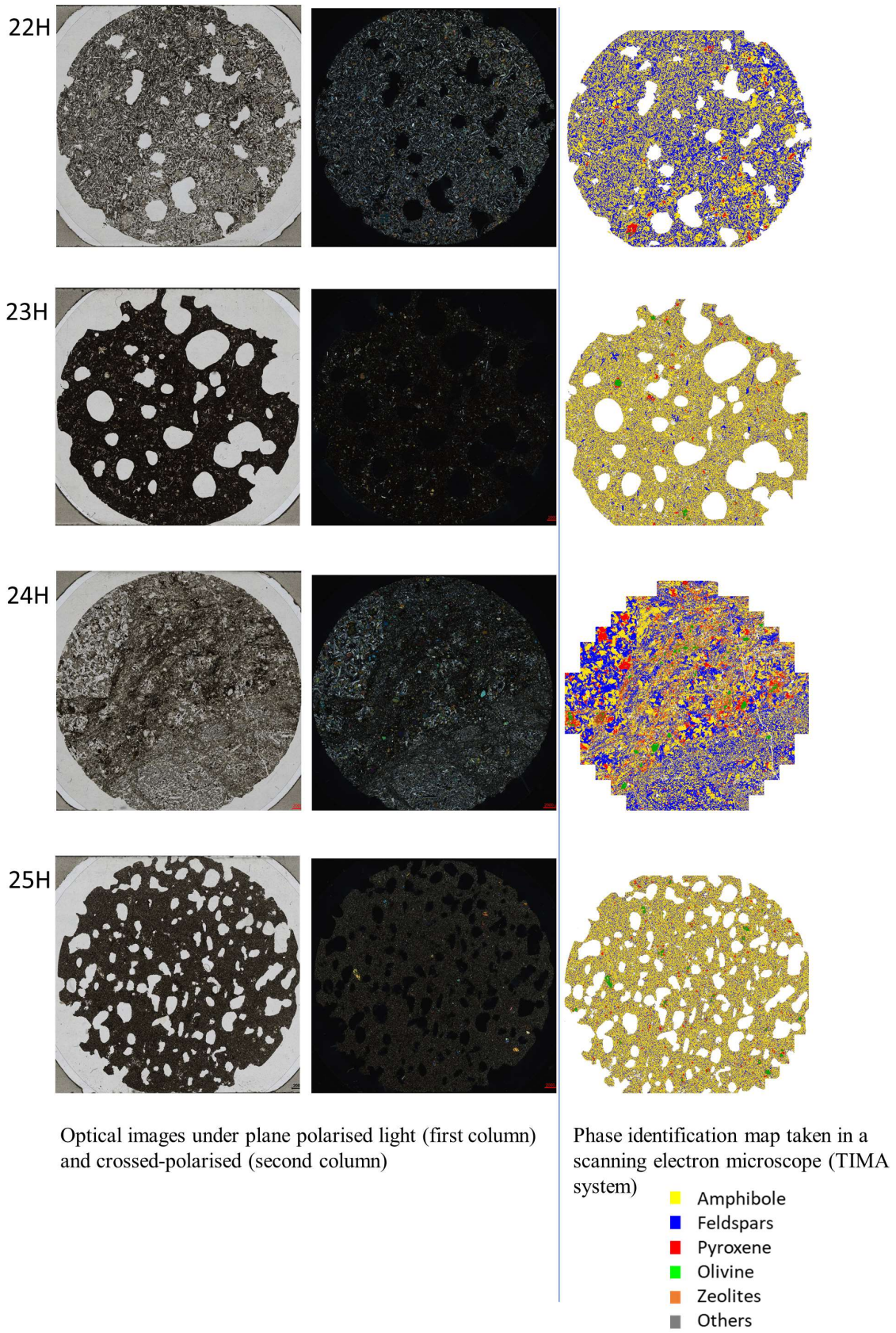

Figure S5. *Thin sections: microscopy scan and mineral mapping*

S6. Mineral distribution per sample

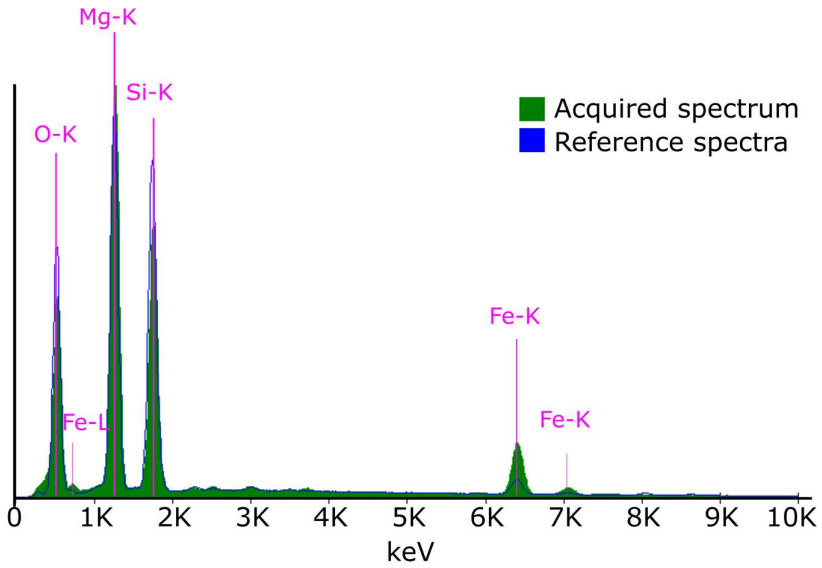

Figure S6. *Phases identification using TIMA. Example for the spectrum of Olivine.*

Table S6.1. *Mass % per phase*

Sample	*Amphibole*	*Feldspars*	*Pyroxene*	*Olivine*	*Zeolites*	*Others*
1H	53.24	42.26	1.36	0.24	0.07	2.83
2H	42.43	38.90	4.17	11.06	0.38	3.06
4H	60.53	28.68	3.61	4.62	0.27	2.29
5H	63.48	32.30	0.48	0.29	0.08	3.37
6H	40.63	28.68	7.16	21.29	0.35	1.89
7H	54.97	25.90	6.29	2.94	8.22	1.69
8H	66.53	29.01	0.53	0.65	0.90	2.37
9H	61.58	32.74	0.17	0.32	2.75	2.45
11H	57.17	36.11	0.38	0.50	3.16	2.67
12H	53.65	36.13	0.42	0.24	6.17	3.38
14H	48.87	40.84	0.66	0.28	5.87	3.48
15H	51.65	36.25	0.72	0.32	7.87	3.20
17H	44.72	24.81	5.38	17.63	5.63	1.82
18H	41.83	30.64	5.63	0.13	19.46	2.31
19H	45.25	22.61	3.26	26.28	0.39	2.21
20H	62.19	33.19	1.42	0.41	0.24	2.55
21H	77.05	19.01	1.58	1.43	0.56	0.37
22H	49.17	42.71	1.46	0.46	0.03	6.16
23H	69.12	26.80	1.32	0.84	0.16	1.76
24H	45.31	39.81	9.58	1.40	0.55	3.35
25H	68.79	25.62	1.78	1.33	0.19	2.28

Table S6.2. *List of shear-wave velocity for mineral groups*.

Mineral	Vs mm/µs
Amphiboles	3.77 [a]
Feldspars	2.39 [b]
Olivine	4.91 [b]
Pyroxene	2.72 [b]
Zeolites	3.50-4.77 [b]

Note. [a]Ji et al. (2013). [b]Mavko et al. (2009)

Table S6.3 *Grain size % per sample*

Midpoint [µm]	*1H*	*2H*	*4H*	*5H*	*6H*	*7H*	*8H*	*9H*	*11H*	*12H*	*14H*	*15H*	*17H*	*18H*	*19H*	*20H*	*21H*	*22H*	*23H*	*24H*	*25H*
3.66	0.10	0.07	0.10	0.11	0.07	0.20	0.57	0.21	0.32	0.13	0.14	0.16	0.08	0.18	0.08	0.04	0.23	0.07	0.14	0.11	0.11
4.44	0.24	0.15	0.22	0.26	0.11	0.31	0.66	0.33	0.62	0.19	0.21	0.22	0.17	0.21	0.22	0.13	0.42	0.17	0.34	0.32	0.28
5.39	0.39	0.24	0.34	0.42	0.16	0.43	0.84	0.47	0.87	0.28	0.32	0.31	0.27	0.27	0.35	0.24	0.55	0.28	0.54	0.50	0.45
6.55	0.45	0.27	0.39	0.52	0.18	0.47	0.89	0.51	0.96	0.31	0.35	0.34	0.29	0.27	0.43	0.28	0.61	0.32	0.61	0.57	0.53
7.95	0.89	0.53	0.74	1.04	0.33	0.90	1.67	1.00	1.90	0.59	0.71	0.64	0.57	0.48	0.85	0.57	1.13	0.63	1.18	1.18	1.03
9.65	1.25	0.71	0.98	1.49	0.44	1.17	2.25	1.36	2.56	0.82	0.99	0.87	0.79	0.60	1.20	0.81	1.47	0.86	1.57	1.74	1.39
11.72	1.67	0.90	1.25	2.06	0.56	1.46	2.99	1.73	3.17	1.08	1.33	1.12	1.04	0.75	1.65	1.08	1.86	1.09	2.00	2.40	1.77
14.23	1.82	0.93	1.23	2.35	0.58	1.43	3.04	1.72	3.04	1.14	1.39	1.23	1.16	0.81	1.80	1.12	2.00	1.15	2.10	2.51	1.79
17.28	2.06	1.13	1.26	2.83	0.70	1.49	3.23	1.79	3.19	1.32	1.58	1.44	1.36	0.99	2.09	1.24	2.41	1.34	2.36	2.62	1.98
20.98	2.59	1.67	1.46	3.70	1.00	1.82	3.77	2.13	3.99	1.77	2.00	1.96	1.74	1.41	2.68	1.57	3.15	1.91	2.98	3.02	2.44
25.48	3.40	3.04	2.37	5.29	1.85	2.66	4.70	2.95	4.96	2.80	2.81	2.95	2.64	2.37	3.82	2.51	4.51	3.17	4.28	3.62	3.64
30.94	4.43	5.34	4.47	6.94	3.50	4.09	6.41	4.63	6.89	4.59	3.79	4.48	4.35	3.73	5.30	5.01	6.62	4.92	6.27	4.31	6.49
37.57	4.48	3.57	3.00	6.90	2.07	3.56	6.41	3.89	7.34	3.18	3.10	3.31	2.92	2.57	4.98	2.86	6.64	4.10	6.45	4.15	5.39
45.62	5.28	4.37	4.24	8.00	2.77	4.64	7.62	5.12	8.21	3.96	3.68	4.06	3.55	3.07	5.94	4.40	7.61	5.00	7.72	4.52	7.14
55.39	6.05	4.54	5.08	8.98	3.08	5.49	8.50	6.05	8.91	4.42	4.32	4.61	3.80	3.25	6.54	5.31	8.36	5.42	8.77	4.62	8.44
67.26	6.55	4.48	5.93	9.53	3.18	6.10	8.99	6.89	8.93	5.18	4.82	5.17	3.95	3.34	6.94	6.36	8.56	5.75	9.39	4.73	9.57
81.68	6.82	5.03	7.82	10.03	3.91	6.78	9.54	7.69	8.48	6.50	5.70	6.11	4.30	3.67	6.96	7.85	8.84	5.95	9.63	4.98	10.42
99.18	6.19	5.47	8.88	9.85	4.50	7.40	8.81	8.43	7.69	7.29	6.65	6.54	4.79	4.00	6.42	9.23	8.97	6.30	8.80	4.85	10.19
120.44	5.08	6.20	10.12	8.16	5.51	7.62	7.38	8.51	6.96	8.75	7.08	7.23	5.10	4.35	5.25	10.45	8.48	6.65	7.59	5.06	9.05
146.25	3.91	7.02	10.48	5.93	6.62	7.29	5.55	8.49	4.82	9.29	7.71	7.30	5.52	4.61	3.97	10.53	7.27	6.95	6.34	5.00	7.44
177.59	3.22	7.27	10.20	3.37	7.52	6.77	3.28	7.44	3.06	9.33	8.10	7.55	6.12	5.48	2.40	10.16	5.04	7.11	4.41	4.79	5.44
215.65	2.52	6.56	8.46	1.54	7.45	5.65	1.87	6.51	1.98	9.17	7.37	7.18	6.87	6.23	1.16	8.45	3.05	6.96	3.22	4.22	2.85
261.87	1.54	6.51	5.27	0.51	6.75	4.82	0.65	5.22	0.65	7.43	7.49	6.97	7.56	6.27	0.82	5.33	1.36	6.74	1.77	4.56	1.49
318.00	1.43	5.86	2.59	0.12	6.52	3.79	0.22	3.67	0.28	5.64	5.94	5.54	6.90	6.69	0.81	2.28	0.59	5.50	0.90	4.55	0.38
386.15	1.47	4.96	1.45	0.07	4.84	3.20	0.17	1.98	0.10	2.62	4.51	4.99	6.93	6.59	1.28	1.12	0.05	4.79	0.32	4.92	0.00
468.91	2.43	3.40	0.82	0.00	4.77	2.48	0.00	0.77	0.14	1.57	2.28	2.90	5.96	6.23	1.64	0.76	0.00	3.13	0.11	4.38	0.17
569.41	4.06	2.75	0.40	0.00	3.46	3.12	0.00	0.49	0.00	0.58	3.00	2.72	3.31	5.84	3.15	0.17	0.00	2.31	0.08	3.51	0.00
691.45	3.68	2.03	0.14	0.00	4.62	1.85	0.00	0.00	0.00	0.08	1.79	1.70	1.87	6.16	3.00	0.13	0.00	1.08	0.13	4.89	0.13
839.64	6.01	0.69	0.00	0.00	4.03	0.96	0.00	0.00	0.00	0.00	0.50	0.16	2.61	5.62	4.22	0.00	0.24	0.36	0.00	1.79	0.00
1019.60	4.50	2.38	0.30	0.00	3.84	1.29	0.00	0.00	0.00	0.00	0.34	0.23	2.32	2.77	3.60	0.00	0.00	0.00	0.00	1.01	0.00
1238.12	4.59	1.01	0.00	0.00	4.55	0.34	0.00	0.00	0.00	0.00	0.00	0.00	1.18	0.90	5.27	0.00	0.00	0.00	0.00	0.55	0.00
1503.48	0.93	0.89	0.00	0.00	0.52	0.41	0.00	0.00	0.00	0.00	0.00	0.00	0.00	0.31	5.21	0.00	0.00	0.00	0.00	0.00	0.00

S7. Statistical parameters

Table S7. *Statistical parameters from the velocity fluctuations in volcanic rock samples*

Sample	*ε %* *Standard deviation of velocity fluctuations*	*a (mm)* *Scale length of heterogeneity*
1H	11.0	0.29
2H	12.5	0.08
4H	8.2	1.19
5H	10.2	0.39
6H	10.5	0.55
7H	11.8	0.22
9H	9.0	0.71
11H	11.1	0.41
12H	8.6	0.61
14H	8.1	0.55
15H	8.4	0.65
18H	11.2	0.14
20H	12.6	0.09
21H	10.3	0.53
22H	12.8	0.25
23H	9.4	0.39
25H	8.7	0.85

S8 – Qc vs frequency content

The ultrasonic experiments were performed using a source transducer with a characteristic frequency of 1 MHz. However, the frequency content on the output signals (seismograms) varies between samples (λ reported in Table S1). The median frequency content in the dataset is 150 kHz. The lowest central frequency recorded was around 70 kHz (sample 19H), while the highest frequency observed was ~350 kHz (sample 3H). The results in the paper correspond to coda attenuation values (Qc^{-1}) computed at a central frequency of 150 kHz for all the samples. Here we re-plot figures 6 and 12 (Fig S8.1 & S8.2 respectively) presenting the attenuation values as a function of the wavelength of each sample. Observing the plots scaled by the wavelength does not change the analysis of the results. We also tested how the frequency affects the coda attenuation by computing Qc values at a range of frequencies from 50 to 400 kHz (Fig. S8.3). As expected, we observe that Qc increases linearly with frequency, the slope of the linear relationship varies at an acceptable level between samples (the minimum slope is 0.23 for sample 14H and the maximum slope is 0.40 for sample 17H).

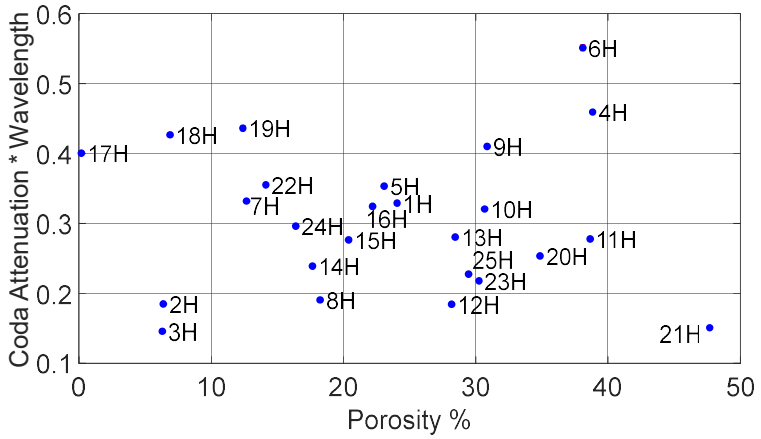

Figure S8.1. *Coda attenuation values computed at a central frequency of 150 kHz and scaled by the wavelength recorded at each sample versus porosity.*

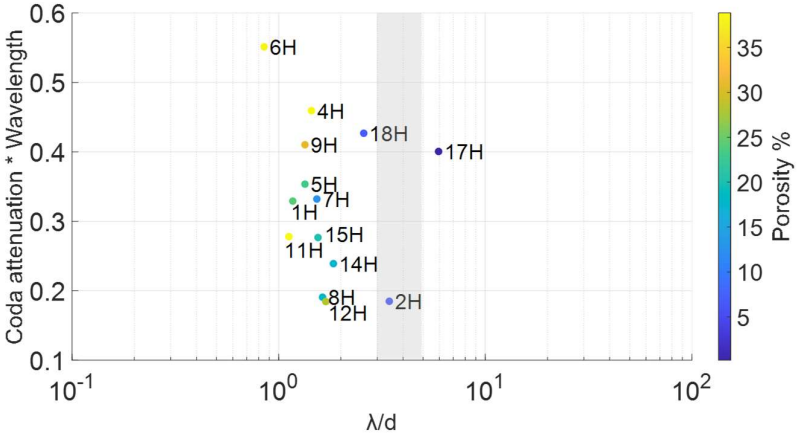

Figure S8.2. *Coda attenuation values computed at a central frequency of 150 kHz and scaled by the wavelength recorded at each sample versus the ratio λ/d (λ: seismic wavelength at 150 kHz, d: the size of heterogeneities related to the equivalent diameter of the pores in the sample).*

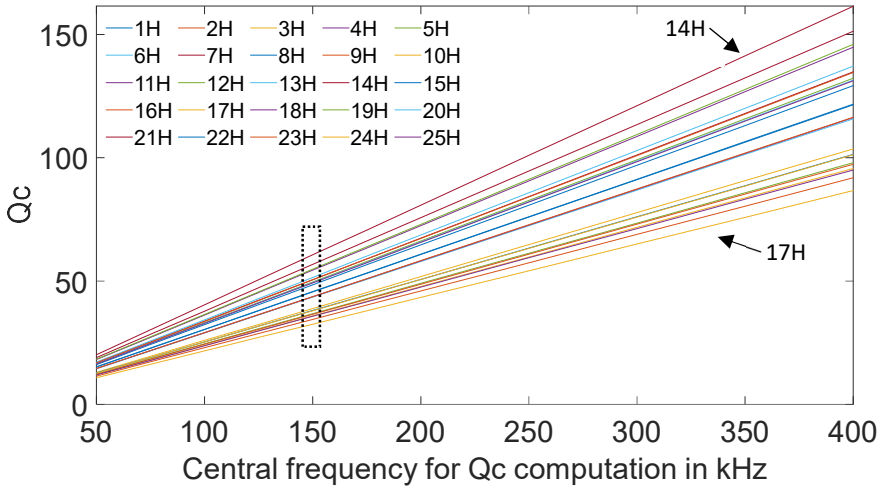

Figure S8.3. *Qc vs central frequency per sample. The dashed box represents the Qc values computed at a central frequency of 150kHz, these are the values used to present the results in the main manuscript.*